Radiation response of multicomponent $L1_2$ γ′ precipitates strengthened high entropy alloys The role of γ/γ′ interface

Huang, Shasha; Fu, Haijun; Xiong, Yaoxu; Lu, Wenyu; Ma, Shihua; Xiang, Xuepeng; Kai, Ji-Jung; Zhao, Shijun

Published in:
Journal of Materials Research and Technology

Published: 01/11/2024

Document Version:
Final Published version, also known as Publisher's PDF, Publisher's Final version or Version of Record

Published version (DOI):
10.1016/j.jmrt.2024.11.249

Publication details:
Huang, S., Fu, H., Xiong, Y., Lu, W., Ma, S., Xiang, X., Kai, J.-J., & Zhao, S. (2024). Radiation response of multicomponent $L1_2$ γ′ precipitates strengthened high entropy alloys: The role of γ/γ′ interface. *Journal of Materials Research and Technology*, *33*, 9289-9296. https://doi.org/10.1016/j.jmrt.2024.11.249

Journal of Materials Research and Technology 33 (2024) 9289–9296

Contents lists available at ScienceDirect

Journal of Materials Research and Technology

journal homepage: www.elsevier.com/locate/jmrt

Radiation response of multicomponent $L1_2$ γ' precipitates strengthened high entropy alloys: The role of γ/γ' interface

Shasha Huang [a], Haijun Fu [a], Yaoxu Xiong [a], Wenyu Lu [a], Shihua Ma [a], Xuepeng Xiang [a,b], Ji-Jung Kai [a], Shijun Zhao [a,*]

[a] Department of Mechanical Engineering, City University of Hong Kong, Hong Kong, China
[b] School of Environment and Energy, South China University of Technology, Guangzhou, 510006, China

ARTICLE INFO

Keywords:
Multicomponent $L1_2$ intermetallics
Interfacial mismatch
Chemical disorder
Defect evolution
Molecular dynamics

ABSTRACT

The advancement of high entropy alloys (HEAs) has stimulated the development of multicomponent $L1_2$ γ' intermetallics, which exhibit both excellent strength and ductility. These intermetallics with long-range order are typically employed as coherent precipitates to enhance the high-temperature performance of HEAs. This study investigates the influence of multicomponent γ' intermetallics on the irradiation response of the strengthened HEA γ phase, focusing on the role of the multicomponent γ/γ' interface in defect production and evolution. Our results indicate that the chemical disorder within the multicomponent γ' phase leads to a broad defect energy spectrum near the interface zone, diminishing its effectiveness as a defect sink. Based on these observations, we propose that, distinct from traditional superalloys, the γ/γ' interface plays a minor role in the irradiation resilience of multicomponent γ' intermetallics-strengthened HEAs. Instead, the inherent chemical disorder within the multicomponent γ' intermetallics emerges as the key factor.

1. Introduction

The advancement in multiprincipal elemental alloys (MPEAs), including high-entropy alloys (HEAs), has marked a revolutionary approach in materials engineering, targeting exceptional mechanical properties and enhanced irradiation resistance [1–6]. In MPEAs, the inherent chemical disorder and resultant lattice distortion can effectively suppress defect kinetics, leading to high strength and promising radiation tolerance [7–12]. However, the application of HEAs faces the challenge of balancing strength and toughness at elevated temperatures [3,13–15]. A promising strategy to augment high-temperature performance involves the incorporation of the $L1_2$ γ' intermetallics, known for their robust mechanical strength and prevalent use as strengthening components in conventional Ni-based superalloys [16–21]. Inspired by MPEAs, the introduction of multi-principal components into the sublattices of γ' intermetallics can significantly increase the anti-phase boundary energy, boosting their strengthening functionality [13]. By carefully selecting appropriate multicomponent intermetallics (MCIs) as precipitates, the properties of MCI-strengthened HEAs can be effectively tailored for high-temperature applications.

Ni-based superalloys find extensive utilization in nuclear reactors due to their outstanding mechanical properties and corrosion resistance [22,23], rendering their irradiation response critical for reactor safety and performance. The beneficial properties of these alloys are primarily attributed to coherent $L1_2$-structured γ' Ni_3Al precipitates dispersed throughout the γ-Ni matrix [24–26]. In such alloys, both the γ phase matrix and γ' intermetallics share a face-centered cubic (FCC) structure, fostering a coherent interface between the matrix and the precipitate, which is essential for strengthening purposes. Under irradiation, the γ/γ' interface, characterized by lattice mismatch due to differing lattice constants between γ and γ' phases, plays a vital role in defect dynamics. The γ' particles often undergo disorder and start dissolving at the interface under irradiation [27–31], impacting phase stability and the irradiation response of the γ'-strengthened superalloys [27,31]. The incorporation of multicomponents into the precipitates causes chemical disordering at the γ/γ' interface, potentially altering elemental arrangement and coherence. Consequently, the interface is anticipated to exert a significant impact on the irradiation response of MCI-strengthened HEAs.

Experiments on MCI-strengthened HEAs reveal a distinct role of γ/γ' interface under irradiation. For instance, MCI-strengthened NiFeCoCr HEA demonstrates a uniform distribution of helium bubbles across both

* Corresponding author.
E-mail address: shijzhao@cityu.edu.hk (S. Zhao).

https://doi.org/10.1016/j.jmrt.2024.11.249
Received 24 September 2024; Received in revised form 14 November 2024; Accepted 26 November 2024
Available online 27 November 2024

γ and γ′ phases, suggesting a minor effect of the chemically disordered γ/γ′ interface [32]. The chemical disorder in MCIs not only affects the degree of mismatch at interfaces but also alters the energy landscape for defect evolution. It has been revealed that partial chemical disorder within the γ′ phase significantly influences defect diffusion properties [33,34]. Specifically, chemical disorder induced by Co atoms in (Ni, Co)$_3$Al has been observed to enhance vacancy diffusion, thus facilitating defect recombinations [33]. Therefore, in MCIs, the chemical disorder may override the role of the interface as defect sinks by modifying defect dynamics.

Building on prior research that underscores the impressive irradiation resistance of L1$_2$-strengthened HEAs, such as (Ni,Co)$_3$(Al,Ti)-strengthened NiFeCoCrAlTi [34], this study examines the role of the γ/γ′ interface in MCI-strengthened HEAs under irradiation. We focus on the effects of interfacial mismatch and chemical disorder, considering several typical γ/γ′ systems, including Ni/Ni$_3$Al, Ni/Ni$_3$Ti, Ni/Ni$_3$(Al,Ti), Ni/(Ni,Co)$_3$Al, and Ni/(Ni,Co)$_3$(Al,Ti), where Co and Ti are critical elements assisting the precipitation of γ′ phase [31,35,36]. Although Co is readily activated by thermal neutrons, it has a low fast neutron absorption cross-section [37], making it viable for use in fast neutron reactors. Additionally, non-equilibrium conditions such as irradiation-enhanced diffusion and irradiation-induced segregations [38,39] significantly promote local chemical ordering within HEAs, which can lead to defect trapping in localized areas, such as pure Ni [40]. In this context, our study models the γ matrix exclusively as pure Ni to streamline the analysis of interfacial mismatch effects. Through molecular dynamics (MD) simulations, we demonstrate that while increasing interfacial mismatch can enhance the ability of the interface to act as a defect sink, the presence of chemical disorder can dilute this effect by generating a rough defect energy landscape near the interface, diminishing the role of interfaces as defect recombination catalysts. This study highlights a strategic balance of interfacial mismatch and chemical disorder for optimizing the irradiation resistance of nano-precipitate strengthened HEAs.

2. Method

MD and molecular statics (MS) simulations were performed using LAMMPS [41]. The Modified Embedded Atom Model (MEAM) developed in our previous work was employed [42]. MD simulations were conducted in a $34a_0 \times 34a_0 \times 34a_0$ FCC supercell [43–45], while a $10a_0 \times 10a_0 \times 20a_0$ FCC supercell was used for MS, where a_0 denotes the lattice constant of the system. In both cases, the supercells were structured such that the upper half contained the γ′ phase and the lower half consisted of pure Ni, with both maintaining coherent {100} crystallographic planes to form the $[100]_{\gamma'}//[100]_{Ni}$ interface. Partial chemical disorder in the L1$_2$ A$_3$B intermetallic was introduced by randomly distributing Ni and Co atoms within the A sublattice, and Al and Ti within the B sublattice, following the stoichiometries of Ni$_3$(Al,Ti), (Ni, Co)$_3$Al, and (Ni,Co)$_3$(Al,Ti), respectively. For cascade simulations, a primary knock-on atom (PKA) with an energy of 5 keV was introduced at various initial distances from the interface and directed towards it to simulate an ion bombardment event. The variable timestep method was applied, dynamically adjusting the timestep to restrict atomic displacements to a maximum of 0.01 Å per step. The total simulation time was approximately 50 ps to allow for the complete cooling of the damage cascade. To prevent boundary effects, the border region (two atomic layers around the simulation cell) was maintained at 300 K through a Nose-Hoover thermostat. The resulting defects were examined using the Wigner-Seitz defect analysis as implemented in the Ovito software [46].

The defects considered in this work include interstitials and vacancies, with their formation energies calculated using $E_f = E - E_0 \pm \mu$, where E and E_0 are the total energies of the supercell with and without defects, respectively, and μ is the chemical potential of the element composed of the defect (energy per atom in the corresponding pure metals). The vacancy migration energy was determined by the climbing-image nudged elastic band (CI-NEB) method [47], with a timestep of 0.01 fs, and a total of 15 intermediate images. The force convergence criterion in NEB calculations was 1×10^{-6} eV/Å. The interfacial mismatch is quantified by $\epsilon = 2\frac{a_+ - a_-}{a_+ + a_-}$ [48], where a_+ and a_- represent the crystal lattice parameters of the upper (γ′) and lower (γ) phases, respectively.

To compare the diffusion properties of interstitials and vacancies across different systems, the trajectory of a single Ni interstitial or a single vacancy within 30 ns is analyzed. Considering the lower mobility of vacancy compared to interstitial, the diffusion of vacancy was examined at 1400 K, whereas that of interstitial was at 1000 K.

3. Results

3.1. Interfacial mismatch

The calculated interfacial mismatches for each considered system are displayed in Table 1. Notably, the interfacial mismatch of the Ni/Ni$_3$Al system corroborates well with previous first-principles calculations and experimental measurements [49–52]. Despite their relatively simple chemical compositions, Ni/Ni$_3$Al and Ni/Ni$_3$Ti show significantly distinct interfacial mismatches, providing a foundation to explore their impact on defect behaviors. Meanwhile, Ni/Ni$_3$(Al,Ti) and Ni/(Ni, Co)$_3$Al have intermediate levels of mismatch, despite their increased chemical complexity. In contrast, Ni/(Ni,Co)$_3$(Al,Ti) exhibits the highest degrees of both chemical complexity and interfacial mismatch among the systems examined.

3.2. Primary damage production and recombination

In our cascade simulations, the PKA was initiated from the Ni side, as illustrated in Fig. 1(a). After a relaxation period of 50 ps, the number of survived defects in both the Ni and γ′ sides was computed. Assuming the defect numbers are n_{Ni} and $n_{\gamma'}$ in the Ni and γ′ phase, respectively, the fraction of defects produced in the mixed system relative to the defects in their respective pure phases was calculated as follows [53]:

$$f_{defect} = \frac{n_{Ni}}{n_{Ni}^{bulk}} + \frac{n_{\gamma'}}{n_{\gamma'}^{bulk}} \quad (2)$$

where n_{Ni}^{bulk} and $n_{\gamma'}^{bulk}$ are the defect numbers produced in the pure Ni and γ′ bulk phases, respectively. The average defect numbers from 200 independent simulations in the pure Ni and the γ′ phases are listed in Table 2. Generally, more defects are observed in the ordered γ′ phase than in pure Ni, likely due to the suppressed defect recombination, consistent with prior research [54].

Based on these numbers, the defect fractions for vacancies (VAC) and interstitials (SIA) as a function of the initial PKA position relative to the interface are depicted in Fig. 1(b)–(f). To ensure accuracy and account for the statistical error, 15 independent cascades were conducted at each PKA distance. The averaged defect fractions offer insights into the defect distribution relative to the pure phases and elucidates the role of the interface. Fig. 1(b)–(f) show that when the PKA is initiated close to the interface, the fractions of vacancies and interstitials are nearly equal, indicating that the coherent interface does not preferentially retain one defect type over the other.

Table 1
Interfacial mismatch (ϵ: %) between Ni and γ′ phases.

	Ni/ Ni$_3$Al	Ni/ Ni$_3$Ti	Ni/Ni$_3$(Al, Ti)	Ni/(Ni, Co)$_3$Al	Ni/(Ni,Co)$_3$(Al, Ti)
(ϵ: %)	1.37	2.10	1.81	2.08	2.14

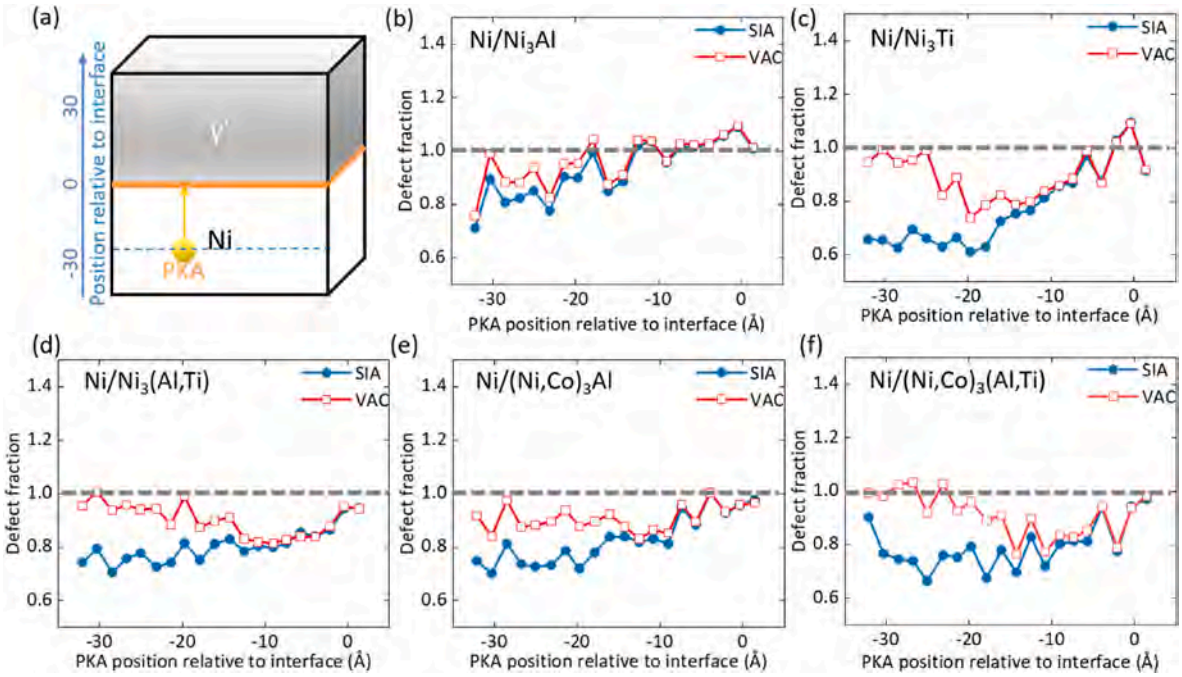

Fig. 1. (a) Schematic illustration of the cascade simulation model. The shadow region represents the γ′ phase, and the yellow ball represents the Ni PKA initiated at different original positions with respect to the interface from the Ni side. The direction of the PKA is toward the interface from Ni to the γ′ phase. Defect fraction produced in (b) Ni/Ni_3Al, (c) Ni/Ni_3Ti, (d) $Ni/Ni_3(Al,Ti)$, (e) $Ni/(Ni,Co)_3Al$, and (f) $Ni/(Ni,Co)_3(Al,Ti)$ as a function of PKA position relative to the interface. (For interpretation of the references to color in this figure legend, the reader is referred to the Web version of this article.)

Table 2
The average number of defects produced (n^{bulk}) in pure Ni and γ′ phase derived from 200 independent 5 keV cascade simulations at 300 K.

	Ni	Ni_3Al	Ni_3Ti	$Ni_3(Al,Ti)$	$(Ni,Co)_3Al$	$(Ni,Co)_3(Al,Ti)$
n^{bulk}	16	20	41	28	28	31

However, when the PKA initiates further from the interface, a distinct difference emerges, with a higher fraction of vacancies compared to interstitials. This disparity arises from the greater mobility of interstitials compared to vacancies at the simulation temperature of 300 K. While vacancies remain predominantly localized near their production sites in the Ni region, the more mobile interstitials are capable of traversing into the γ′ phase. Quantitative analysis, as shown in Table 2, demonstrates that the γ′ phase consistently exhibits a higher average defect concentration than pure Ni. According to Eq. (2), the migration of interstitials into the γ′ phase results in a reduced defect count of $n_{\gamma'}$ compared to defects generated directly within the γ′ phase. This movement of interstitials between the two phases leads to a reduction in f_{defect}. Conversely, vacancies are more likely to stay near their formation locations, displaying fractions close to unity except in areas where interface effects are pronounced.

The defect fraction value in the mixed system serves as an indicator of defect recombination. Particularly, $f_{defect} < 1$ suggests that the interface enhances defect recombination compared to pure phases, while a value close to 1 implies the minimal impact of the interface on recombination. The analysis of Fig. 1(b) and (c) reveals that a higher interfacial mismatch in Ni/Ni_3Ti enhances defect recombination, especially when the cascade core region is close to the interface (with PKA position about 15 Å from the interface). In contrast, the Ni/Ni_3Al interface exhibits a much weaker influence, as evidenced by the near-one f_{defect} values consistently.

The interfacial mismatch in $Ni/Ni_3(Al,Ti)$ and $Ni/(Ni,Co)_3Al$ is stronger than that in Ni/Ni_3Al, leading to more efficient defect recombination, as illustrated in Fig. 1(d) and (e). Despite $Ni/(Ni,Co)_3(Al,Ti)$ having the most severe interfacial mismatch among the systems studied, its defect behavior is similar to that of $Ni/Ni_3(Al,Ti)$ and $Ni/(Ni,Co)_3Al$. Compared to Ni/Ni_3Ti, $Ni/(Ni,Co)_3(Al,Ti)$ demonstrates a weaker interface effect on defect annealing, suggesting that the incorporation of chemical disorder may diminish the impact of interfacial mismatch on defect evolution. Nevertheless, for all the MCIs, f_{defect} values remain below one, indicating that the interfaces, despite their reduced effect, still help to decrease defect numbers relative to pure phases. This aligns with observations from previous studies showing defect suppression in HEAs with γ′ phase [32,55,56].

3.3. Defect energetics

To further explore the interplay between interfacial mismatch and chemical disorder observed in Fig. 1, we compare the defect formation energies in Ni/Ni_3Al, Ni/Ni_3Ti, and $Ni/(Ni,Co)_3(Al,Ti)$ by manually introducing a single <100> dumbbell or vacancy into the $10a_0 \times 10a_0 \times 20a_0$ FCC supercell. Here, Ni/Ni_3Al and Ni/Ni_3Ti were selected for their differing interfacial mismatches but similar chemical disorder, providing a contrast in structural but not compositional complexity. Conversely, $Ni/(Ni,Co)_3(Al,Ti)$ was chosen for its interfacial mismatch similar to that of Ni/Ni_3Ti, yet featuring distinct chemical disorder, allowing us to isolate and evaluate the effects of chemical complexity on defect formation energies.

Fig. 2(a)–(c) provide the formation energies of <100> dumbbell, while Fig. 2(d)–(f) present the vacancy formation energies relative to the interface position. Given the chemical complexity of $Ni/(Ni,Co)_3(Al,Ti)$, 100 independent calculations were conducted to obtain the average E_f, along with error bars indicating the standard error in Fig. 2(c) and (f). In $L1_2$ unit cells, two inequivalent Ni sites at the same (001) plane result in distinct E_f for Ni-containing dumbbells. The results of interstitial formation energies reveal lower values in the γ′ phase, aligning with the preference for interstitials in this phase, as discussed in Fig. 1.

In Ni/Ni_3Al, the vacancy formation energies remain consistent across the interface, as demonstrated in Fig. 2(d). Notably, Fig. 2(e) indicates a significant decrease in vacancy formation energies from the Ni side to

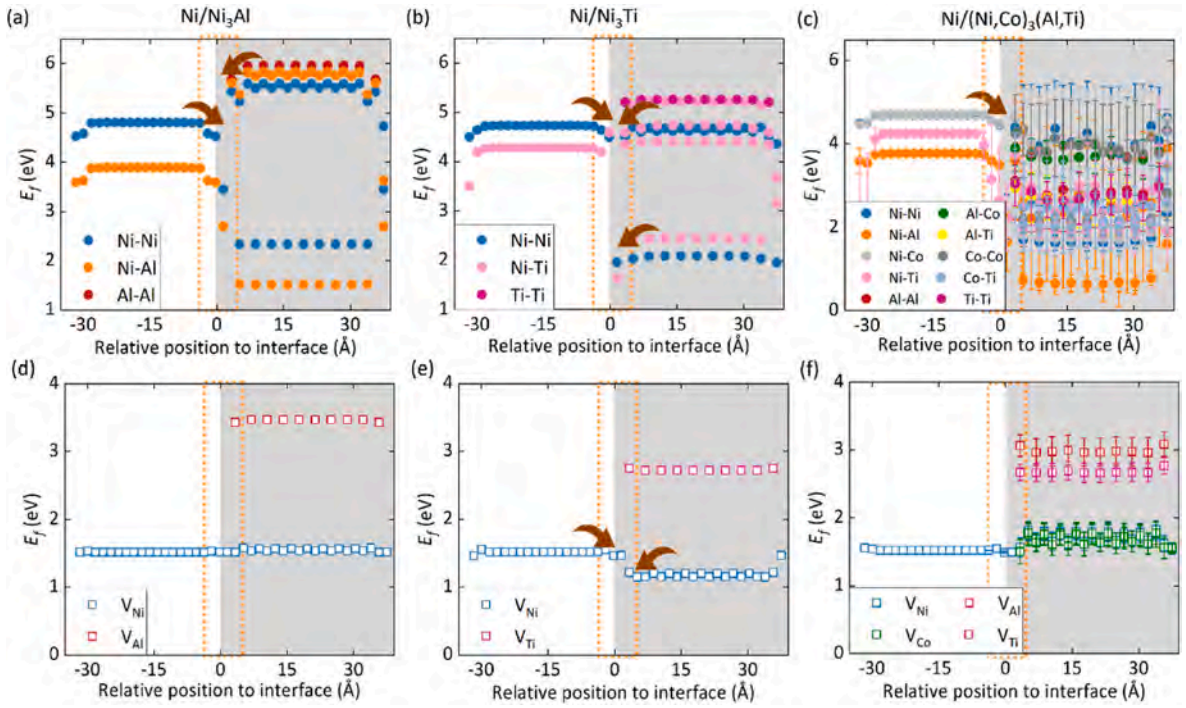

Fig. 2. Formation energies of a <100> dumbbell in (a) Ni/Ni_3Al, (b) Ni/Ni_3Ti, and (c) $Ni/(Ni,Co)_3(Al,Ti)$; and of a vacancy in (d) Ni/Ni_3Al and (e) Ni/Ni_3Ti, and (f) $Ni/(Ni,Co)_3(Al,Ti)$ as a function of the relative position to the interface. The shadow regions represent the γ′ phase, and the brown arrows highlight the trends in formation energy near the interface. (For interpretation of the references to color in this figure legend, the reader is referred to the Web version of this article.)

the γ′ side in Ni/Ni_3Ti, with both sides reaching minimum values at the interface (highlighted by the brown arrows around the orange dashed box). This trend is mirrored for interstitials, suggesting that the severe interfacial mismatch improves the role of the Ni/Ni_3Ti interface as a defect sink, enhancing defect annihilation, as observed in Fig. 1(b).

Despite a similar interfacial mismatch to Ni/Ni_3Ti, the presence of chemical disorder in $Ni/(Ni,Co)_3(Al,Ti)$ introduces a diverse local chemical environments, resulting in a broader range of defect formation energies in both γ′ side and interface region, as illustrated by the energy distributions in Fig. 1(c) and (f). Consequently, unlike in Ni/Ni_3Ti, where vacancies and interstitials encounter consistently low-energy sites at the interface, the broad energy distribution around the interface region of $Ni/(Ni,Co)_3(Al,Ti)$ decreases the likelihood of defects being captured and annihilated. This diminished defect-sink effectiveness highlights the impact of chemical disorder on defect behavior at the interface.

3.4. Defect dynamics

In addition to defect formation energies, defect dynamics play a critical role in determining how defects interact with interfaces [54,57]. To capture these dynamics, we calculated vacancy migration barriers in different zones, including the γ′ side, the interface zone, and the Ni side. Owing to the crystalline symmetry in Ni/Ni_3Al and Ni/Ni_3Ti, there are three different migration paths in γ′ side and interface zone, respectively. In contrast, 25 independent NEB calculations were performed in $Ni/(Ni,Co)_3(Al,Ti)$ in each zone (Fig. 3(c)) to consider the chemical complexity. The average migration energies in different zones are also indicated in Fig. 3.

In the Ni/Ni_3Al system, the vacancy migration energy increases from the Ni side to the interface, followed by a slight decrease on the γ′ side. However, in Ni/Ni_3Ti, the vacancy migration energy is significantly reduced at the interface zone, suggesting enhanced defect transport through the Ni/Ni_3Ti interface. The $Ni/(Ni,Co)_3(Al,Ti)$ system, characterized by higher chemical complexity, displays similar migration energy distributions in the interface zone and γ′ phase, indicating a diminished interfacial effect.

Our cascade simulation results in Fig. 1 indicate that interstitials tend to migrate towards the γ′ phase. To further understand the mechanism, we directly simulated the diffusion behavior of a single Ni interstitial or vacancy in the three interface-containing systems. Given that vacancies diffuse slowly at low temperatures, the diffusion temperature was set to

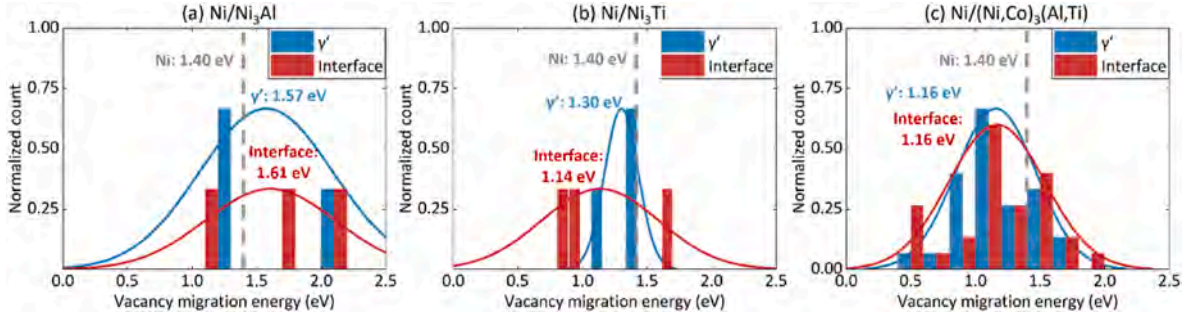

Fig. 3. Vacancy migration energies in (a) Ni/Ni_3Al, (b) Ni/Ni_3Ti, and (c) $Ni/(Ni,Co)_3(Al,Ti)$. The average migration energies in different zones were also shown in the figure.

1400 K for vacancies and 1000 K for interstitials to accelerate the simulation process. Fig. 4 depicts the trajectories of the z-coordinate (the normal direction to the interface) of the defects.

In these simulations, defects were initialized at three distinct locations: (i) in the γ′ phase (red dots), (ii) near the interface (green dots), and (iii) in the Ni phase (blue dots). To account for statistical variability, three independent simulations were conducted for vacancies at each initial position (represented by different shades of color). In the Ni/Ni_3Al system, vacancies slightly favor the Ni phase, while all interstitials gravitate towards the Ni_3Al side. The divergence in their trajectories diminishes the probability of mutual interaction with the interface, resulting in a defect fraction close to one for all cases examined (Fig. 1 (b)).

In contrast, both vacancies and interstitials in the Ni/Ni_3Ti system show a preference for residing within the Ni_3Ti phase, irrespective of their initial positions. The concurrent diffusion of both vacancies and interstitials toward the γ′ phase increases their likelihood of mutual interaction with the interface. This behavior facilitates defect recombination around the interface, consistent with the lower than one defect fraction value observed in the Ni/Ni_3Ti system (as shown in Fig. 1(c)).

In the Ni/$(Ni,Co)_3(Al,Ti)$ system, the reduced difference in vacancy migration barriers between the interface and the γ′ phase diminished the role of interface in vacancy migration. Furthermore, the rough energy landscape induces local trapping of vacancies, causing them to oscillate near the interface. Examination of Fig. 4(d)–(f) reveals that interstitials in Ni/$(Ni,Co)_3(Al,Ti)$ are confined to a more restricted area away from the interface than Ni/Ni_3Al and Ni/Ni_3Ti, possibly due to the broad distribution of interstitial formation energies, with interstitials preferentially occupying locations of lower formation energy. The attenuated tendency for vacancy transport into the γ′ phase, coupled with reduced interstitial-interface interactions, resulted in a slightly diminished capacity of the interface to promote defect recombination than Ni/Ni_3Ti.

Although the diffusion trajectories were simulated at only one temperature for each defect type, the results in Fig. 4 indicate that their preferences for different regions at high temperatures are strongly influenced by their formation energies and migration energy barriers at 0 K. This suggests that the energy landscape, rather than temperature, plays a more dominant role in determining their behavior, indicating that the observed diffusion patterns may be broadly applicable at other temperatures.

The above findings confirm that in both Ni/Ni_3Al and Ni/Ni_3Ti, interstitials generated by irradiation favor the γ′ side, while the behavior of vacancies is influenced by the energy landscape. The pronounced interfacial mismatch can enhance the sink effect, promoting more efficient vacancy migration and potentially enhancing defect recombination at the interface. However, in Ni/$(Ni,Co)_3(Al,Ti)$, chemical disorder reduces the transport of vacancies into the γ′ phase, while simultaneously reducing interstitial-interface interactions. This trend implies that chemical disorder may diminish the impact of interfacial mismatch, potentially reducing the effectiveness of the interface in aiding defect migration and recombination.

3.5. Defect evolution at kinetic stage

The prior single cascade simulation allows for the simultaneous observation of how interfaces affect defect generation and recombination, primarily resulting from interstitial diffusion. To further explore how interfacial mismatch and chemical disorder influence defect evolution involving vacancies, we introduced Frenkel pairs (FPs) by randomly displacing atoms within the cells at a defect concentration of 0.5%. Their clustering and diffusion behaviors were then monitored over 1 ns at 1000 K using the NVT ensemble.

Fig. 5 showcases the defect configurations at the end of the simulations. Despite the initially uniform distribution of defects, interstitials rapidly concentrated in the γ′ side, expediting the recombination of FPs and reducing the number of vacancies in γ′ side, leading to the separated distribution of interstitials and vacancies. However, the mismatched interfaces significantly enhanced vacancy transport and facilitated recombination, notably decreasing the defect density near the Ni/Ni_3Ti interface and forming a nearly denuded zone, as marked by grey dashed box in Fig. 5(b). This effect was less evident in Ni/Ni_3Al due to its weaker mismatch. In the more chemically complex Ni/$(Ni,Co)_3(Al,Ti)$, despite a higher mismatch than Ni/Ni_3Ti, a broader energy spectrum reduced the effectiveness of interface as a defect sink, leading to a diminished

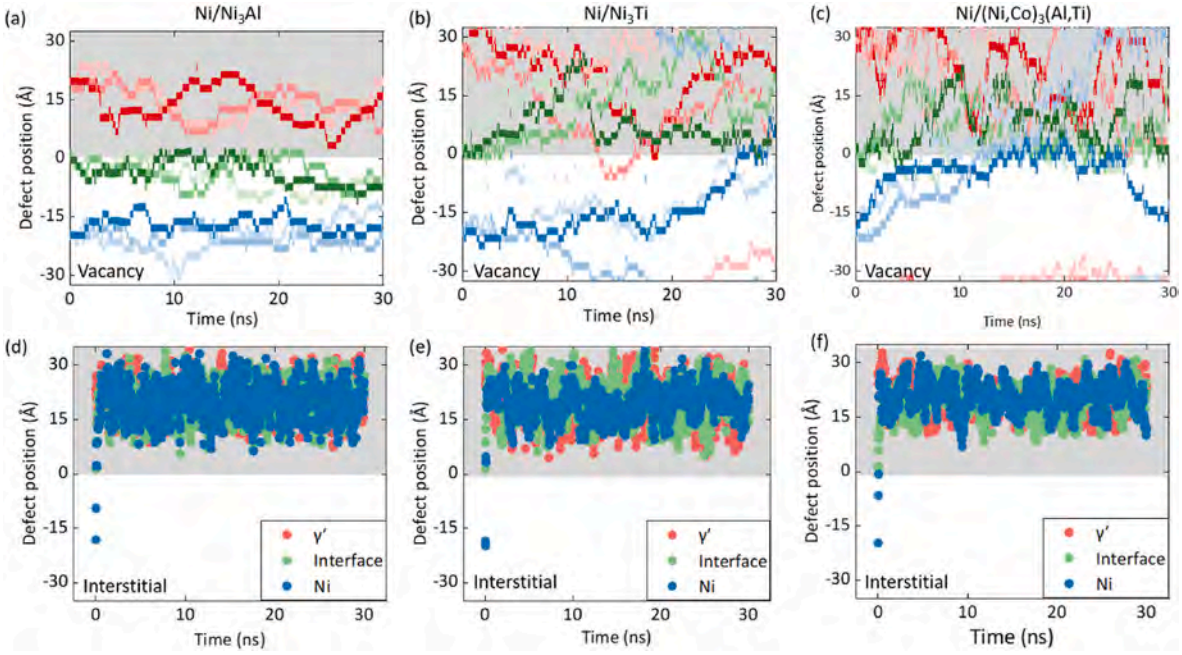

Fig. 4. Trajectories of the *z* coordinate (normal direction to the interface) for a vacancy in (a) Ni/Ni_3Al, (b) Ni/Ni_3Ti, and (c) Ni/$(Ni,Co)_3(Al,Ti)$; and for an interstitial in (d) Ni/Ni_3Al, (e) Ni/Ni_3Ti, and (f) Ni/$(Ni,Co)_3(Al,Ti)$. The shadow region represents the γ′ phase. Vacancy diffusion is simulated at 1400 K, whereas that of interstitial is at 1000 K.

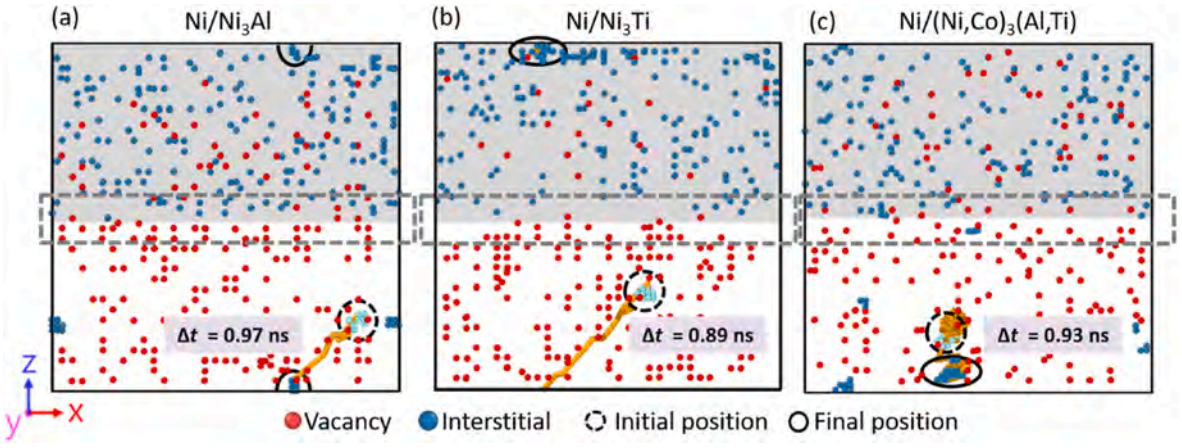

Fig. 5. Defect configuration and trajectory of interstitial clusters in (a) Ni/Ni_3Al, (b) Ni/Ni_3Ti, and (c) $Ni/(Ni,Co)_3(Al,Ti)$ at the end of the simulation ($t = 1$ ns). The shadow region represents the γ' phase. The initial position of the interstitial cluster when it was formed is encircled by black dashed circles, while its final position is shown by solid circles. The trajectory of the cluster is illustrated by orange lines. The duration of each trajectory is also indicated in the figure. (For interpretation of the references to color in this figure legend, the reader is referred to the Web version of this article.)

interface effect than Ni/Ni_3Ti.

The weakened interface effect by chemical complexity can also be observed from the diffusion trajectories of interstitial clusters. In all three cases, interstitial clusters migrated towards the interface, consistent with previous experimental observations of interstitial clusters formation at interfaces [29,58]. Fig. 5(a) and (b) illustrate a more pronounced attractive effect at the highly mismatched Ni/Ni_3Ti interface than the Ni/Ni_3Al interface, whereas the trajectories in $Ni/(Ni,Co)_3(Al,Ti)$ were more erratic, suggesting that chemical disorder suppresses the defect-interface interaction. Notably, the migration duration of the cluster towards the Ni/Ni_3Ti interfaces is the shortest, as indicated by the values of 0.89 ns. This fast migration suggests strong defect-interface coupling in this system. In contrast, the longer duration of 0.93 ns in $Ni/(Ni,Co)_3(Al,Ti)$ reflects more diffusive and less directed migration behavior, further elucidating that chemical disorder weakens the interaction between defects and the interface.

4. Discussion

In reality, the incorporation of $L1_2$ γ' intermetallics effectively enhances the high-temperature strength of HEAs [16–19], but the inherent chemical complexity of HEAs often leads to chemical disorder within these intermetallics. This disorder, along with lattice mismatches between the γ' phase and the matrix, significantly affects how interfaces interact with defects, thereby influencing the irradiation response of precipitate-strengthened HEAs [59–61]. Our analysis of traditional γ' phases (Ni_3Al and Ni_3Ti) shows that an increased interfacial mismatch promotes vacancy migration and interstitial absorption at the interface, enhancing FPs recombination, at least at the initial stage of irradiation damage when irradiation-induced ballistic mixing is dominant. These findings aligned with previous studies show that Ni_3Ti-strengthened superalloys exhibit a higher threshold dose for disordering compared to those strengthened with Ni_3Al at similar temperatures [30,42,62,63]. Nonetheless, the appearance of chemical disorder broadens the defect energy spectrum around the interface, thereby diminishing its effectiveness in annihilating defects. A schematic illustration of these processes is provided in Fig. 6. Although the HEA matrix in this study is simplified as Ni, the presence of multiple principal elements in HEAs generally creates a complex energy landscape that can trap defects in local regions. Consequently, similar weakening effects of interfaces are expected, consistent with the uniform distribution of defects found in nanoparticle-strengthened HEAs [32,34,64,65], thus suggesting a broader applicability of our findings across diverse HEA systems.

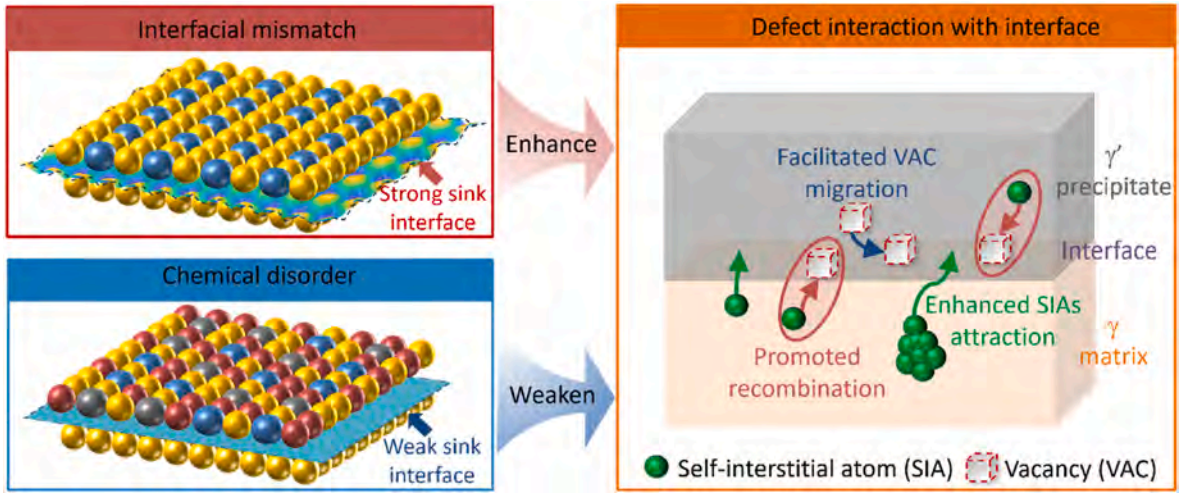

Fig. 6. Schematic illustration of the influence of interfacial mismatch and chemical disorder on defect evolution in γ/γ' system.

5. Conclusion

In summary, we investigate the irradiation response of multicomponent intermetallics-strengthened HEAs, focusing on the role of the γ/γ' interface. Through atomistic simulations, we assess how interfacial mismatch and chemical disorder impact defect production and evolution. Our results show that a highly mismatched interface acts as an effective defect sink, enhancing defect recombination. However, the introduction of chemical disorder reduces the effectiveness of interfaces by creating a broadly distributed energy spectrum, even in the presence of significant mismatch. This study thus highlights the complex interplay between interfacial mismatch and chemical disorder in MCI-strenghened HEAs, revealing their nuanced impact on material resilience under irradiation.

Declaration of competing interest

The authors declare that they have no known competing financial interests or personal relationships that could have appeared to influence the work reported in this paper.

Acknowledgment

This work was supported by the Research Grant Council of Hong Kong (Nos. C1017-21G and C7074-23G). The computational time provided by the CityU Burgundy Supercomputer is highly acknowledged.

References

[1] Chuang M-H, Tsai M-H, Wang W-R, Lin S-J, Yeh J-W. Microstructure and wear behavior of AlxCo1.5CrFeNi1.5Tiy high-entropy alloys. Acta Mater 2011;59:6308–17.
[2] Ma SG, Zhang Y. Effect of Nb addition on the microstructure and properties of AlCoCrFeNi high-entropy alloy. Mater Sci Eng A 2012;532:480–6.
[3] Wu Z, Bei H, Pharr GM, George EP. Temperature dependence of the mechanical properties of equiatomic solid solution alloys with face-centered cubic crystal structures. Acta Mater 2014;81:428–41.
[4] Lu C, Niu L, Chen N, Jin K, Yang T, Xiu P, et al. Enhancing radiation tolerance by controlling defect mobility and migration pathways in multicomponent single-phase alloys. Nat Commun 2016;7:13564.
[5] Yeh JW, Chen SK, Lin SJ, Gan JY, Chin TS, Shun TT, et al. Nanostructured high-entropy alloys with multiple principal elements: novel alloy design concepts and outcomes. Adv Eng Mater 2004;6:299–303.
[6] Granberg F, Nordlund K, Ullah MW, Jin K, Lu C, Bei H, et al. Mechanism of radiation damage reduction in equiatomic multicomponent single phase alloys. Phys Rev Lett 2016;116:135504.
[7] Zhao S, Osetsky Y, Barashev AV, Zhang Y. Frenkel defect recombination in Ni and Ni–containing concentrated solid–solution alloys. Acta Mater 2019;173:184–94.
[8] Zhang Y, Zhao S, Weber WJ, Nordlund K, Granberg F, Djurabekova F. Atomic-level heterogeneity and defect dynamics in concentrated solid-solution alloys. Curr Opin Solid State Mater Sci 2017;21:221–37.
[9] Egami T, Guo W, Rack P, Nagase T. Irradiation resistance of multicomponent alloys. Metall Mater Trans A 2014;45:180–3.
[10] Zhao S, Osetsky Y, Zhang Y. Preferential diffusion in concentrated solid solution alloys: NiFe, NiCo and NiCoCr. Acta Mater 2017;128:391–9.
[11] Jin K, Lu C, Wang LM, Qu J, Weber WJ, Zhang Y, et al. Effects of compositional complexity on the ion-irradiation induced swelling and hardening in Ni-containing equiatomic alloys. Scr Mater 2016;119:65–70.
[12] Yang T-n, Lu C, Velisa G, Jin K, Xiu P, Zhang Y, et al. Influence of irradiation temperature on void swelling in NiCoFeCrMn and NiCoFeCrPd. Scr Mater 2019;158:57–61.
[13] Zhang J, Ma S, Xiong Y, Xu B, Zhao S. Elemental partitions and deformation mechanisms of L12-type multicomponent intermetallics. Acta Mater 2021;219:117238.
[14] Stiller K, Hättestrand M, Danoix F. Precipitation in 9Ni–12Cr–2Cu maraging steels. Acta Mater 1998;46:6063–73.
[15] Geddes B, Leon H, Huang X. Superalloys: alloying and performance. Asm International; 2010.
[16] Reed R, Rae C. Physical metallurgy of the nickel-based superalloys. Physical Metallurgy. Elsevier; 2014. p. 2215–90.
[17] Ferasat K, Swinburne TD, Saidi P, Daymond MR, Yao Z, Béland LK. Interstitialcy-based reordering kinetics of Ni3Al precipitates in irradiated Ni-based super alloys. Materialia. 2021;19:101180.
[18] Hou JX, Liu SF, Cao BX, Luan JH, Zhao YL, Chen Z, et al. Designing nanoparticles-strengthened high-entropy alloys with simultaneously enhanced strength-ductility synergy at both room and elevated temperatures. Acta Mater 2022;238:118216.
[19] Zhao YL, Yang T, Li YR, Fan L, Han B, Jiao ZB, et al. Superior high-temperature properties and deformation-induced planar faults in a novel L12-strengthened high-entropy alloy. Acta Mater 2020;188:517–27.
[20] Pollock TM, Tin S. Nickel-based superalloys for advanced turbine engines: chemistry, microstructure and properties. J Propul Power 2006;22:361–74.
[21] Reed RC. The superalloys: fundamentals and applications. Cambridge university press; 2008.
[22] Wang F, Liu Y, Yang Q, Ma D, Li D. Microscale stray grains formation in single-crystal turbine blades of Ni-based superalloys. J Mater Sci Technol 2024;191:134–45.
[23] Griffiths M. Ni-based alloys for reactor internals and steam generator applications. Structural alloys for nuclear energy applications. Elsevier; 2019. p. 349–409.
[24] Kovarik L, Unocic RR, Li J, Sarosi P, Shen C, Wang Y, et al. Microtwinning and other shearing mechanisms at intermediate temperatures in Ni-based superalloys. Prog Mater Sci 2009;54:839–73.
[25] Smith TM, Good BS, Gabb TP, Esser BD, Egan AJ, Evans LJ, et al. Effect of stacking fault segregation and local phase transformations on creep strength in Ni-base superalloys. Acta Mater 2019;172:55–65.
[26] Chen C, Meng F, Song J. Planar fault transformation and unfaulting of interstitial dislocation loops in irradiated L12-Ni3Al. Scr Mater 2024;242:115898.
[27] Potter D, Hoff H. Irradiation effects on precipitation in γγ' Ni Al alloys. Acta Metall 1976;24:1155–64.
[28] Potter DI, Ryding DG. Precipitate coarsening, redistribution and renucleaton during irradiation of Ni-6.35 wt.% Al. J Nucl Mater 1977;71:14–24.
[29] Sun C, Maloy SA, Baldwin K, Wang Y, Valdez JA. Phase stability of Ni/Ni3Al multilayers under thermal annealing and irradiation. J Occup Med 2020;72:3995–4001.
[30] Yeli G, Chen D, Yabuuchi K, Kimura A, Liu S, Lin W, et al. The stability of γ' precipitates in a multi-component FeCoNiCrTi0. 2 alloy under elevated-temperature irradiation. J Nucl Mater 2020;540:152364.
[31] Yang T, Guo W, Poplawsky JD, Li D, Wang L, Li Y, et al. Structural damage and phase stability of Al0.3CoCrFeNi high entropy alloy under high temperature ion irradiation. Acta Mater 2020;188:1–15.
[32] Feng T, Jiang S, Hu X, Zhang Z, Huang Z, Dong S, et al. Evolution of helium bubbles in FeCoNiCr-based high-entropy alloys containing γ'nanoprecipitates. Chin Phys B 2024.
[33] Zhao S, Osetsky Y. Structural and chemical disorder enhance point defect diffusion and atomic transport in Ni3Al-based γ' phase. Acta Mater 2021;207:116704.
[34] Zhao Y, Meng F, Yang T, Luan J, Liu S, Yeli G, et al. Enhanced helium ion irradiation tolerance in a Fe-Co-Ni-Cr-Al-Ti high-entropy alloy with L12 nanoparticles. J Mater Sci Technol 2023;143:169–77.
[35] Mazey D, Hanks W.The effect of Si, Al and Ti additions on the void swelling response of ion-irradiated PE16-base alloy. Materials for nuclear reactor core applications 2 v1987.
[36] Chen D, Zhao S, Sun J, Tai P, Sheng Y, Yeli G, et al. Effects of minor alloying addition on He bubble formation in the irradiated FeCoNiCr-based high-entropy alloys. J Nucl Mater 2020;542:152458.
[37] Spencer R, Macklin R. Neutron capture cross section of cobalt-59 in the energy range 2.5 to 1000 keV. Nucl Sci Eng 1976;61:346–55.
[38] Huang S, Zhang J, Xiong Y, Ma S, Xu B, Zhao S. Effects of local chemical ordering on defect evolution in NiFe concentrated solid solution alloy. J Nucl Mater 2022;568:153877.
[39] Barashev A, Osetsky Y, Bei H, Lu C, Wang L, Zhang Y. Chemically-biased diffusion and segregation impede void growth in irradiated Ni-Fe alloys. Curr Opin Solid State Mater Sci 2019;23:92–100.
[40] Lu C, Yang T, Jin K, Gao N, Xiu P, Zhang Y, et al. Radiation-induced segregation on defect clusters in single-phase concentrated solid-solution alloys. Acta Mater 2017;127:98–107.
[41] Plimpton S. Fast parallel algorithms for short-range molecular dynamics. J Comput Phys 1995;117:1–19.
[42] Huang S, Xiong Y, Ma S, Zhang J, Fu H, Xu B, et al. Enhancing the irradiation resistance of L12 intermetallics by incorporating multiple principal elements through computational modeling. J Mater Res Technol 2024;30:9274–84.
[43] Zhao S. Fluctuations in stacking fault energies improve irradiation tolerance of concentrated solid-solution alloys. J Nucl Mater 2020;530:151886.
[44] Vörtler K, Juslin N, Bonny G, Malerba L, Nordlund K. The effect of prolonged irradiation on defect production and ordering in Fe–Cr and Fe–Ni alloys. J Phys Condens Matter 2011;23:355007.
[45] Zhao S. On the role of heterogeneity in concentrated solid-solution alloys in enhancing their irradiation resistance. J Mater Res 2020;35:1103–12.
[46] Stukowski A. Visualization and analysis of atomistic simulation data with OVITO–the Open Visualization Tool. Model Simulat Mater Sci Eng 2009;18:015012.
[47] Henkelman G, Uberuaga BP, Jónsson H. A climbing image nudged elastic band method for finding saddle points and minimum energy paths. J Chem Phys 2000;113:9901–4.
[48] Romanov A, Wagner T, Rühle M. Coherent to incoherent transition in mismatched interfaces. Scr Mater 1998;38:869–75.
[49] Woodward C, van de Walle A, Asta M, Trinkle DR. First-principles study of interfacial boundaries in Ni–Ni3Al. Acta Mater 2014;75:60–70.
[50] Pearson WB. A handbook of lattice spacings and structures of metals and alloys: international series of monographs on metal physics and physical metallurgy, vol. 4. Elsevier; 2013.
[51] Simmons G. Single crystal elastic constants and caluculated aggregate properties. A handbook 1971;4.

[52] Prikhodko SV, Yang H, Ardell AJ, Carnes JD, Isaak DG. Temperature and composition dependence of the elastic constants of Ni3Al. Metall Mater Trans A 1999;30:2403–8.
[53] Xu H, Si S, Li Y, Liu X, Li W, Jiang C, et al. The effect of Laves phase on heavy-ion radiation response of Nb-containing FeCrAl alloy for accident-tolerant fuel cladding. Fundam Res 2022;2:437–46.
[54] Zhao S, Chen D, Yeli G, Kai JJ. Atomistic insight into the effects of order, disorder and their interface on defect evolution. J Alloys Compd 2021;859:157770.
[55] Cao PP, Wang H, He JY, Xu C, Jiang SH, Du JL, et al. Effects of nanosized precipitates on irradiation behavior of CoCrFeNi high entropy alloys. J Alloys Compd 2021;859:158291.
[56] Zheng Y, Lu W, Qian F, Jia N, Dou Y, He X, et al. Self-ion irradiation response of (CoCrFeNi)94Ti2Al4 alloy containing coherent nanoprecipitates. J Nucl Mater 2021;549:152889.
[57] Chen H, Wang L, Peng F, Xu Q, Xiong Y, Zhao S, et al. Hydrogen retention and affecting factors in rolled tungsten: thermal desorption spectra and molecular dynamics simulations. Int J Hydrogen Energy 2023;48:30522–31.
[58] Zhu H, Qin M, Aughterson R, Wei T, Lumpkin G, Ma Y, et al. The formation and accumulation of radiation-induced defects and the role of lamellar interfaces in radiation damage of titanium aluminum alloy irradiated with Kr-ions at room temperature. Acta Mater 2020;195:654–67.
[59] Han W, Demkowicz MJ, Mara NA, Fu E, Sinha S, Rollett AD, et al. Design of radiation tolerant materials via interface engineering. Adv Mater 2013;25:6975–9.
[60] Kato T, Nakata K, Masaoka I, Takahashi H, Takeyama T, Ohnuki S, et al. The irradiation-induced microstructural development and the role of γ' on void formation in Ni-based alloys. J Nucl Mater 1984;122:721–6.
[61] Yang Z, Qiu N, Yang H, Chen Q, Wang Y. Irradiation tolerance enhanced by coherent interfaces of FCC/BCC HEA multilayers. Surf Coat Technol 2023;457:129338.
[62] Müller S, Abromeit C, Matsumura S, Wanderka N, Wollenberger H. Disordering kinetics of Ni3Al under ion irradiation. J Nucl Mater 1999;271–272:241–5.
[63] Bourdeau Camus, Abromeit Wollenberger. Disordering and dissolution of gamma ' precipitates under ion irradiation. Phys Rev, B Condens 1994;50(22):16205–11.
[64] Chen D, Tong Y, Wang J, Han B, Zhao YL, He F, et al. Microstructural response of He+ irradiated FeCoNiCrTi0.2 high-entropy alloy. J Nucl Mater 2018;510:187–92.
[65] Ardell AJ, Mastel B, Laidler JJ. High-voltage electron irradiation studies of several overaged γ/γ' alloys. J Nucl Mater 1974;54:313–24.